Comparison of SCM and CSRM Forcing Data Derived from the ECMWF Model and from Objective Analysis at the ARM SGP Site

Shaocheng Xie[1], Richard T. Cederwall[1], Minghua Zhang[2], J. John Yio[1]

[1]Lawrence Livermore National Laboratory, Livermore, CA

[2]State University of New York, Stony Brook, NY

Submitted to: Journal of Geophysical Research

Submission Date:

Manuscript No:

Received:

Corresponding author address: Dr. Shaocheng Xie, L-103, ASD, Lawrence Livermore National Laboratory, Livermore, CA 94550. Tel. 925-422-6023.

Abstract. The large-scale forcing data diagnosed from the ECMWF model for driving Single-Column Models (SCMs) and Cloud System Resolving Models (CSRMs) are compared with forcing data derived using objective variational analysis constrained by observations collected at the ARM Southern Great Plains (SGP). The comparison covers three different synoptic conditions: a strong precipitation period dominated by sub-grid scale processes during the ARM summer 1997 Intensive Operational Period (IOP), a moderate precipitation period dominated by synoptic scale processes during the Spring 2000 IOP, and a non-precipitation period during the Fall 2000 IOP. In the study, we demonstrate that the ECMWF diagnosed forcing fields are reasonable overall during the moderate and non-precipitation periods while they show considerably large differences from those derived from the ARM objective analysis during the strong convective precipitation period. By analyzing the column-integrated heat and moisture budgets, we show that errors in the ECMWF model-derived forcing are closely associated with errors in the model predicted surface precipitation, which largely reflect deficiencies of model parameterizations. In SCM tests, we show that SCM simulations are sensitive to the prescribed large-scale forcing and some important SCM simulated fields, such as surface precipitation, tend to follow the ECMWF model simulations rather than the observations when it is forced with the ECMWF forcing.

1. Introduction

The Single-Column Model (SCM) and Cloud System Resolving Model (CSRM) are useful tools to test and evaluate physical parameterizations used in climate models [Randall et al., 1996]. A successful SCM or CSRM test requires highly accurate large-scale forcing data, such as the large-scale advective tendencies of temperature and moisture and vertical velocity. These forcing data can be derived from the data collected in major field programs (e.g., ARM[1] and TOGA-COARE[2]) through objective analysis. However, the observations are often available only over a limited time periods and regions. Over regions and periods where observations are not available or data density is low, the large-scale forcing data are usually obtained from output of operational numerical weather prediction (NWP) models. A potential use of the NWP products is to develop long-term continuous forcing datasets for statistical studies of SCM and CSRM results that are not possible with observations. The NWP forcing has been used in some recent SCM studies [e.g., Iacobellis et al., 2002]. A problem in using the NWP data is that the forcing data themselves are affected by deficiencies of the model physical parameterizations used in generating the data. However, how much model physical parameterizations influence these forcing fields and how the forcing data affect SCM results have not been discussed previously in the literature.

In this paper, we attempt to address the above issues through assessment of the forcing data diagnosed from the European Center for Medium Range Weather Forecast (ECMWF) model by using data collected from the ARM Intensive Operational Periods (IOPs) and processed by the ARM objective variational analysis [Zhang et al., 2001]. We will also present results from SCM tests to demonstrate impacts of using NWP forcing on SCM simulations.

2. Large-scale forcing

[1] Atmospheric Radiation Measurement program.

2.1. Observed forcing

The large-scale forcing data, such as the large-scale advective tendencies and vertical motion, cannot be observed directly from field measurements. They are derived from the field observations by using objective analysis methods. The objective analysis scheme used in this study is the constrained variational analysis approach developed in Zhang and Lin [1997]. The variational analysis approach uses the domain-averaged surface precipitation, latent and sensible heat fluxes, and radiative fluxes at the surface and the Top of the Atmosphere (TOA) as the constraints, to enforce the atmospheric state variables to satisfy the conservation of mass, heat, moisture and momentum. Therefore, the derived dataset from this approach is dynamically and thermodynamically consistent. Zhang et al. [2001] showed that the constrained variational analysis could significantly reduce the sensitivity of the final analyzed products to the input observations. Other studies have also shown that this approach significantly improves the accuracy of the large-scale forcing and therefore its derived forcing datasets have been used in several SCM and CSRM studies [e.g., Ghan et al., 2000; Xie et al., 2002; Xu et al., 2002]. Fig. 1 displays the variational analysis domain that is circled by the analysis grids (•), which includes the five ARM sounding stations (∗) and seven wind profiler stations (◇) near the ARM Southern Great Plains (SGP) site.

2.2. ECMWF forcing

ECMWF has been providing ARM with continuous datasets including the large-scale forcing data, covering all three ARM field research sites: North Slope of Alaska (NSA), SGP, and Tropical Western Pacific (TWP) since 1995. The model forcing is specifically extracted from the ECMWF model runs to force SCMs. These data are averaged over an area that is close to the ARM variational analysis domain (see Fig. 1). The dataset is a composite of 12 to 36 hour forecasts. The model used to generate the dataset is the ECMWF global spectral model. Detailed information can be found in the release notice for the SGP ECMWF data sets

---

[2] Tropical Ocean-Global Atmosphere Coupled Ocean-Atmosphere Response Experiment.

at: www.arm.gov/docs/xds/static/ecmwf.html. Information about the model physical parameterizations can be seen in Gregory et al. [2000].

3. Analysis

In this study, a strong precipitation period from 23 June (2330 UTC) to 29 June (2330 UTC) during the Summer 1997 IOP, a moderate precipitation period from 8 March (1730 UTC) to 18 March (1730 UTC) during the Spring 2000 IOP, and a non-precipitation period from 27 Nov. (1730 UTC) to 3 Dec. (1730 UTC) during the Fall 2000 IOP are selected to assess the ECMWF derived forcing under different weather conditions. All observations are collected at the ARM SGP site.

3.1. Summer strong precipitation case

This case contained two strong precipitation events on day 1 and day 5 and a weak precipitation event on day 3 (Fig. 2, solid line). These precipitation events were associated with mesoscale convective systems and were dominated by sub-grid scale precipitation [Xie et al. 2002]. It is seen that the ECMWF model fails to correctly simulate the strong summertime continental precipitation events (see dotted line in Fig. 2). It largely underestimates the observed precipitation and tends to trigger convection earlier than the observations. Note that strong convective events are generally associated with large-scale dynamic processes of upward motion and low-level moisture convergence. The failure to correctly reproduce the observed precipitation events, which is likely related to deficiencies of the model cumulus parameterization, could have large impact on the diagnosed vertical velocity and advective tendencies as discussed later.

To assess the ECMWF diagnosed forcings, we first examine the column-integrated heat and moisture budgets:

$$Cp\frac{\partial < T >}{\partial t} + Cp < \nabla \cdot \vec{V}T >= R_{TOA} - R_{SRF} + LP_{rec} + SH + L\frac{\partial < q_l >}{\partial t} \qquad (1)$$

$$\frac{\partial < q >}{\partial t} + < \nabla \cdot \vec{V} q > = E_s - P_{rec} - \frac{\partial < q_l >}{\partial t} \qquad (2)$$

where

$$< X > = \frac{1}{g} \int_{p_t}^{p_s} (X) dp$$

In the above, $\vec{V}$ is the wind, T is the temperature, q is the mixing ratio of water vapor, p_s is the surface pressure, p_t is the tropopause pressure, ql is the cloud liquid water content, R is the net downward radiative flux at TOA and at the surface (SRF), P_{rec} is precipitation, L is the latent heat of vaporization, C_p is the heat capacity, SH is the sensible heat flux, and E_s is the surface evaporation. Note that the terms on the right-hand side of the equations are the constraints used in the variational analysis. These constraints are not changed in the analysis.

Table 1 lists the statistics of the observed (values in parenthesis) and model calculated column heat and moisture budget components during the strong convective period. The observed values are obtained from the variational analysis. In the table, 'mean' represents an a time average over the strong convective period, 'std' represents standard deviation, 'rmse' is Root-Mean-Square (RMS) error, and 'corr' is the correlation coefficient. Since cloud liquid term is very small compared to other terms, it is not shown in the table. The budget check shows that the column-integrated energy and moisture budgets are balanced in the constrained variational analysis. The area-averaged ECMWF model data also conserve well the column energy and moisture budgets with an time averaged budget imbalance of about 1.45 W m^{-2} and -1.28W m^{-2}, respectively (not shown in the table).

It is seen from the table that significant disagreements exist between the model and the observations. The model largely overestimates the column net radiative cooling and surface evaporation while it significantly underestimates the surface precipitation (L*PREC) and sensible heat flux. The largest error is in precipitation. The calculated latent heating associated with precipitation shows a bias of approximately 65% of the observed mean, because of the large error in the model predicted surface precipitation. The RMS error of this term is also very large and is similar to the magnitude of the temporal variability in the

observations. Its correlation coefficient with the observations is rather small (0.2). It should be noted that these constraint variables used in the variational analysis are obtained directly from the observations and are not changed during the variational analysis. Therefore, the discrepancies shown in these constraint terms reflect the model simulation errors that are closely related to deficiencies of the model parameterizations.

Consistent with above discussions, the model diagnosed forcing fields, i.e., the column-integrated heat and moisture convergences ($C_p*\langle\nabla\cdot\vec{\boldsymbol{V}}\boldsymbol{T}\rangle$ and $L*\langle\nabla\cdot\vec{\boldsymbol{V}}\boldsymbol{q}\rangle$), are largely different from those derived from the objective variational analysis. It is seen that the variational analysis shows very strong advective cooling and large moisture convergence during the strong convective period, which agree with many observations, while the model exhibits rather weak advective cooling and weak divergence, instead of convergence, in the moisture budget. The magnitudes of the temporal variability in these two ECMWF diagnosed fields are much weaker than those in the variational analysis data. The RMS errors are large, similar to the observed standard deviations, and the correlation coefficients are quite small (0.23 and 0.34, respectively).

It is noted that the heat and moisture storage terms $C_p*\partial\langle\boldsymbol{T}\rangle/\partial\boldsymbol{t}$ and $L*\partial\langle\boldsymbol{q}\rangle/\partial\boldsymbol{t}$ are noticeably differences between the model and the observations, even though the model time averaged temperature and moisture agree well with the observations with errors of less than 0.5 K in temperature and 0.3 g kg^{-1} in moisture, respectively.

Another noteworthy feature is that, for the variational analysis during the convective period, the latent heating associated with precipitation and the advective cooling are the two largest terms to balance each other in the energy budget, and the surface precipitation and the horizontal moisture convergence are the two largest terms to balance each other in the moisture budget. For the model, however, the latent heating is balanced by the column net radiative cooling, and the surface precipitation and the horizontal moisture divergence are balanced by the surface evaporation. The relationships presented in the model calculated

column-integrated budgets of heat and moisture during the strong convective events are often not supported by observations.

Although there are large disagreements between the model and the observations, it is interesting to see that the model calculated column net radiation, sensible heat flux, and evaporation terms show rather high correlation (above 0.9) with the observations. This is mainly because these processes are largely dominated by the strong solar diurnal variations over the midlatitude land in the summer.

The time-height distributions of the derived vertical velocity and the total advective tendencies of temperature and moisture from the variational analysis are shown in Figs. 3a-c for the strong convective period. Note that the total advection of temperature includes the adiabatic expansion/compression term. Corresponding to the observed surface precipitation events (Fig. 2), the derived forcings show strong large-scale advective cooling (associated with strong upward motion) in the middle and upper troposphere and strong moisture convergence in the lower troposphere.

Figs. 4a-c are the same as Figs. 3a-c except for the model derived forcing fields. It is seen that the model derived forcing fields are closely associated with its calculated precipitation. As we showed earlier, however, the calculated precipitation events are much weaker than the observations and also are triggered too early. Associated with these problems, the model derived forcing fields are much weaker compared to those derived from the variational analysis. For some periods, such as on day 1, in which a strong convective event was observed, the two different forcings are even out of phase. On this day, the objectively analyzed data show very strong upward motion and advective cooling in the middle and upper troposphere and large lower-level moisture convergence while the ECMWF data displays weak downward motion and small advective heating in the middle and upper troposphere and weak lower-level moisture divergence.

3.2 Spring moderate precipitation case

The Spring precipitation period contained one single-day precipitation on day 1 and one multi-day precipitation event on days 6-9 (Fig. 5, solid line). In comparison with the Summer case, the Spring precipitation events were relatively weaker and were mainly dominated by large-scale stratiform clouds. It is seen that the ECMWF model is able to generally capture well most of the precipitation events while it underestimates the multi-day precipitation event and trigger the first precipitation event a little earlier (Fig. 5, dotted line).

The statistics of the model calculated column heat and moisture budget components during the precipitation period of the Spring 2000 IOP are listed in Table 2. The corresponding components from the variational analysis are shown in parenthesis. In Comparison with Table 1, the agreements of the model calculated budget components with the observations are much better for the Spring case. The model typically shows high correlation with the observations except for those precipitation related terms such as the latent heating and moisture convergence, where the correlation coefficients are below 0.80. It is seen that both the model and the variational analysis show moisture convergence and horizontal advective cooling during these precipitation periods. The RMS error for these constraint terms is less than the magnitude of the temporal variability in the observations. In terms of the mean value, however, the model overestimates the observed column radiative cooling and surface evaporation and underestimates the surface precipitation and sensible heat flux. Discrepancies in the mean diagnosed heat and moisture convergences are also quite large.

Figures 6a,b display the derived large-scale vertical motions from the variational analysis and the ECMWF model for the Spring case, respectively. The model derived vertical motions agree well overall with those derived from the variational analysis. The larger disagreements are seen on days 7-8 where the model underestimates the observed upward motion and overestimates the downward motion. This is clearly related to the underestimation of the observed precipitation that occurred on those days by the model (see Fig. 5). Another noticeable feature in the figure is that the model overestimates the observed upward/downward motions in the upper troposphere. This might be because the TOA is set to

10 hpa in the ECMWF model while it is set to 100 hpa in the variational analysis. Similar results can be seen in the derived temperature and moisture forcing fields (not shown).

3.3. Fall non-precipitation case

Table 3 lists the statistics of the model calculated and observed column heat and moisture budget components for the non-precipitation period of the Fall 2000 IOP. Similar to the Spring case, the disagreements of the model calculated budget components from the observations are significantly reduced for the non-precipitation case in comparison with the Summer strong convection case. The calculated column net radiative cooling agrees well with the observation, with error less than 7% of the observed value. The model-produced spurious precipitation is very small (0.83 w m^{-2} ~ 0.03 mm day^{-1}) and can be neglected. In contrast, relatively larger errors are seen in the surface evaporation.

For the diagnosed heat and moisture convergences, the model-derived fields show similar temporal variability as those in the variational analysis data. The correlation coefficients are 0.94 and 0.88, respectively, which are even higher than those in the Spring case. Yet, discrepancies in the mean diagnosed heat and moisture convergences are still noticeably large.

Another noticeable feature in Table 3 is that both the model and the variational analysis show that the decrease in the heat storage is balanced by the advective heating and column radiative cooling, and the decrease in the moisture storage is balanced by the moisture divergence and surface evaporation, in absence of precipitation.

Figures 7a,b are the same as Figs. 6a,b except for the non-precipitation period. Both the observations and the model show that large-scale downward motion dominates this non-precipitation period. In general, the model captures well the observed vertical velocity field even though the downward motions are somewhat overestimated.

4. SCM simulations

The NCAR CCM3 SCM with a modified cumulus convection scheme [Xie and Zhang, 2000] is used to investigate impacts of the different large-scale forcings derived from the ARM objective variational analysis and the ECMWF model on SCM simulations. In the SCM runs, the large-scale total advective tendencies of temperature and moisture are specified from these derived forcing fields. The surface forcing is calculated by the model surface parameterizations. To prevent the problem that SCM simulations could drift away from observations over long time integration, a 36-hour forecast of the SCM is launched every day. For each forecast, the temperature and moisture are initialized with the observations. A composite of 12-36 hour forecasts from the series of 36-hour runs is analyzed.

Figures 8a,b respectively give the simulated temperature and moisture biases averaged over the selected strong convective period during the summer 1997 IOP. It is seen that the SCM forced by the two different forcing data produces quite different results. For temperature, the SCM with the ECMWF forcing generally produces a colder atmosphere in the upper troposphere in comparison with the variational analysis forcing. This is related to the weaker forcing derived from the ECMWF (Fig. 4), which results in weaker convection in the SCM. The differences are also large in the lower troposphere where the SCM with the ECMWF-derived forcing shows cold biases while the SCM with the variational analysis forcing produces warm biases. For moisture, the SCM forced by the NWP-derived forcing shows larger dry biases.

The simulated surface precipitation rates by the SCM are shown in Fig. 9 for the strong convective case. The SCM driven by the variational analysis forcing generally reproduces well the observed precipitation. In contrast, the SCM with the ECMWF forcing largely underestimates the observed precipitation. It actually regenerates well the ECMWF model predicted precipitation with the correlation coefficient about 0.72 while the correlation with the observations is only 0.21. Similar results can be found in other fields, such as the TOA longwave and shortwave radiative fluxes and surface latent and sensible heat fluxes. For all

these fields, the SCM with the ECMWF forcing shows higher correlation with the corresponding ECMWF simulations than the observations.

The analysis presented above for the strong convective period highlights a problem when using the forcing derived from NWP models to run SCMs. Problems explored from such SCM tests may not really reflect problems in the tested parameterizations. It may be just because the enforced NWP-derived forcing does not correctly capture the large-scale dynamic features in the observations due to impacts from imperfect model parameterizations that are used to generate the forcing data.

The problem that the SCM with the NWP-derived forcing tends to follow the model simulations rather than the observations is also shown in the Spring precipitation case. Fig. 10 compares the SCM simulated surface precipitation rates with the observed values and the ECMWF predicted values. It is seen that the SCM with the variational analysis forcing captures well the observed precipitation both in magnitude and phase while the SCM with the NWP-derived forcing regenerates well the ECMWF precipitation (correlation is 0.93).

Figures 11 and 12 respectively shows the simulated temperature and moisture biases averaged over the Spring case and the Fall case. It is interesting to see that the SCM with the NWP-derived forcing produces smaller temperature biases at the levels above 765 hpa in comparison with the variational analysis forcing and their differences are relatively large in the lower troposphere and the near surface for both temperature and moisture. The differences in the Fall case show quite different failures. This indicates that the SCM is sensitive to the differences in these two forcing data sets and they cannot be effectively discriminated by the imperfect SCM employed.

5. Discussions and Conclusions

The large-scale forcing dataset diagnosed from the ECMWF model has been assessed under different weather conditions using data collected at the ARM SGP site during three IOPs. Over the strong convective period during the summer 1997 IOP, we have shown that

the ECMWF diagnosed forcing fields are much weaker than those derived from the ARM objective variational analysis. The correlation between these two different forcing data sets is very small. We have shown that these are closely related to the errors in the ECMWF model predicted surface precipitation. The errors in the model predicted surface latent and sensible heat fluxes, and surface and TOA radiative fluxes also influence the diagnosed forcing fields because they are the important components in the column-integrated budgets of heat and moisture. Over the moderate precipitation during the spring 2000 IOP and the non-precipitation period during the Fall 2000 IOP, the disagreements between these two forcing data sets are significantly smaller compared to those over the strong summer convective period. The two forcing data sets display high correlation, although differences between the ECWMF diagnosed data and the variational analysis data are still noticeable.

It is noticed from Fig. 1 that the ECMWF domain is slightly larger than the variational domain. So one cannot expect the domain- averaged forcing fields derived from ECMWF to be exactly the same as those from the variational analysis. However, the significant disagreements between these two types of forcing data shown during the convective period in this study cannot be easily explained by the differences in the size of averaging domains. In fact, an additional check for the ECMWF diagnosed forcing data averaged over a smaller domain shows very similar results.

Another concern for this comparison is that the objective analysis derived large-scale forcing fields may contain sub-grid scale information. This concern can be somewhat alleviated in this study because the variational analysis approach is intended to de-alias small-scale features from the instantaneous soundings by using the domain-averaged constraints to diagnose the desired large-scale forcing fields. However, this approach cannot de-alias data in time and in the vertical direction. In the variational analysis, we have implemented vertical smoothing and time filtering techniques to reduce impacts of the small-scale noise on the derived large-scale forcing variables.

It has been shown that SCM simulations are sensitive to differences in these two different forcing data sets. The SCM with the ECMWF forcing tends to reproduce some important

aspects of the ECMWF model simulated atmosphere (e.g., surface precipitation and radiative fluxes), rather than the observations. This is a worrisome problem for SCM tests because such test results may be misleading.

It should be noted that SCMs and CSRMs have stringent requirements for the large-scale forcing data. This study shows that the forcing data diagnosed from ECWMF data are generally reasonable over the periods that are dominated by large-scale processes (e.g., the Spring case and the Fall case). Over strong convective periods, however, the model diagnosed forcing data show rather large disagreements with the variational analysis forcing and therefore the use of the model derived forcing data should be avoided. The ECMWF model nevertheless provides unique long-term continuous data set, including comprehensive information about the dynamical and physical fields, and there is no doubt that they are very useful for evaluation and development of parameterizations in climate models and understanding the structure of large-scale systems and budgets.

Acknowledgements. This research was performed under the auspices of the U. S. Department of Energy by the University of California, Lawrence Livermore National Laboratory under contract No. W-7405-Eng-48. Work at SUNY Stony Brook was supported by ARM grant DE-FG02-98ER62570 and was also supported by NSF under grant ATM9701950. We thank Dr. Christian Jakob, formerly of ECWMF and now Australian Bureau of Meteorology Research Centre, for valuable discussions and comments on the early version of the manuscript. The ECMWF forcing data are obtained from the ARM data archive and provided by Dr. Christian Jakob.

References

Ghan, S. J., et al., An intercomparison of single column model simulations of summertime midlatitude continental convection. *J. Geophys. Res.*, *105*, 2091-2124, 2000.

Gregory, D., J.-J. Morcrette, C. Jakob, A. M. Beljaars, and T. Stockdale, Revision of convection, radiation and cloud schemes in the ECMWF Integrated Forecasting System. *Q. J. R. Meteorol. Soc*., *126*, 1686-1710, 2000.

Iacobellis, S. F., R. C. J. Somerville, Sensitivity of Radiation Fluxes and Heating Rates to Cloud Microphysics. *The Twelfth ARM Science Team Meeting Proceedings, St. Petersburg, Florida*, 2002.

Randall, D. A., K-M. Xu, R. J. C. Somerville and S. Iacobellis, Single-column models and cloud ensemble models as links between observations and climate models. *J. Climate*, 9, 1683-1697, 1996.

Xie, S. C., and M. H. Zhang, Impact of the convective triggering function on single-column model simulations. *J. Geophys. Res.*, *105*, 14983-14996, 2000.

Xie, S. C., et al., Intercomparison and evaluation of cumulus parameterizations under summertime midlatitude continental conditions. *Q. J. R. Meteorol. Soc*., *128*, 1095-1135, 2002.

Xu, K.-M. et al., An intercomparison of cloud-resolving models with the Atmospheric Radiation Measurement summer 1997 Intensive Observation Period data. *Q. J. R. Meteorol. Soc*., *128*, 593-624, 2002

Zhang, M. H., and J. L. Lin, Constrained variational analysis of sounding data bases on column-integrated budgets of mass, heat, moisture, and momentum: Approach and application to ARM measurements. *J. Atmos. Sci., 54*, 1503-1524, 1997

Zhang, M. H., J. L. Lin, R. T. Cederwall, J. J. Yio, and S. C. Xie, Objective analysis of ARM IOP Data: Method and sensitivity. *Mon. Weather Rev., 129*, 295-311, 2001.

Figure Captions

Figure 1. The boundary locations of the ARM SCM variational analysis domain (•) and the ECMWF analysis domain (×). Symbols ∗ and ◇ represent the locations of the balloons and the wind profilers, respectively.

Figure 2. Time series of the observed (solid) and ECMWF model produced (dotted) surface precipitation rates (mm day^{-1}) during the selected strong precipitation period in 1997 Summer IOP.

Figure 3. The time-height distributions of the derived (a) vertical velocity, (b) total advective tendency of temperature, and (c) total advective tendency of moisture during the selected strong precipitation period in 1997 Summer IOP. Contour interval is 3. Contours greater than 3 or less than -3 are shaded. In these figures, solid lines are for contours greater than or equal to zero and dotted lines for contours less than zero.

Figure 4. Same as Figure 3 except for the ECMWF-derived forcing fields.

Figure 5. Same as Figure 2 except for the selected moderate precipitation period in 2000 Spring IOP.

Figure 6. The time-height distributions of the derived vertical velocity from (a) variational analysis and (b) the ECMWF model for the selected moderate precipitation period in 2000 Spring IOP. Contour interval is 5. Contours greater than 5 or less than -5 are shaded. In these figures, solid lines are for contours greater than or equal to zero and dotted lines for contours less than zero.

Figure 7. Same as Figure 6 except for the selected non-precipitation period in 2000 Fall IOP.

Figure 8. The time-averaged (a) temperature and (b) moisture biases produced from the SCM forced by the ARM variational analysis forcing (solid) and the ECMWF-derived forcing (dashed) over the strong convective period in 1997 Summer IOP.

Figure 9. The time series of the observed (solid), ECMWF produced (solid line with filled circle), and the SCM simulated surface precipitation rates (mm day^{-1}) over the strong convective period in 1997 Summer IOP. Dotted line is for using the ARM variational forcing and dotted line with unfilled circle for using the ECMWF forcing.

Figure 10. Same as Figure 9 except for the selected moderate precipitation period in 2000 Spring IOP.

Figure 11. Same as Figure 8 except for the selected moderate precipitation period in 2000 Spring IOP.

Figure 12. Same as Figure 8 except for the selected non-precipitation period in 2000 Fall IOP.

Table 1. Comparison of ECMWF model data to the ARM observations (values in parenthesis) for the column-integrated heat and moisture budget components during the strong convective period (w m^{-2}).

	Mean	Std	rmse	corr
R_{TOA}-R_{SRF}	-97.7(-57.1)	127. 9 (162.1)	63.8	0.97
L*PREC	90.8 (261.8)	163.6 (517.4)	533.3	0.20
SH	27.8 (40.8)	76.9 (46.6)	42.4	0.90
L*E_s	146.5 (109.6)	151.3 (111.9)	64.1	0.96
$C_p*\partial\langle \boldsymbol{T}\rangle/\partial \boldsymbol{t}$	13.7 (33.6)	284.1 (247.6)	165.9	0.81
$C_p*\langle \nabla\cdot\vec{\boldsymbol{V}}\boldsymbol{T}\rangle$	8.8 (210.7)	254.5 (519.4)	608.7	0.23
$L*\partial\langle \boldsymbol{q}\rangle/\partial \boldsymbol{t}$	11.8 (26.5)	271.1 (225.6)	329.7	0.11
$L*\langle \nabla\cdot\vec{\boldsymbol{V}}\boldsymbol{q}\rangle$	42.6(-178.6)	355.5 (519.4)	558.6	0.34

Table 2. Same as Table 1 except for the Spring precipitation case

	Mean	std	rmse	corr
R_{TOA}-R_{SRF}	-87.7(-71.5)	352.5 (423.5)	40.9	0.96
L*PREC	64.0 (124.3)	131.9 (221.3)	156.7	0.77
SH	29.9 (40.3)	89.0 (76.6)	38.2	0.91
L*E_s	48.3 (30.9)	49.0 (36.3)	30.5	0.87
$C_p*\partial\langle \boldsymbol{T}\rangle/\partial \boldsymbol{t}$	-21.9 (-24.5)	282.1 (263.9)	116.1	0.91
$C_p*\langle \nabla\cdot\vec{\boldsymbol{V}}\boldsymbol{T}\rangle$	39.6 (116.7)	352.5 (423.5)	204.3	0.90
$L*\partial\langle \boldsymbol{q}\rangle/\partial \boldsymbol{t}$	28.0 (3.1)	243.4 (177.1)	154.3	0.78
$L*\langle \nabla\cdot\vec{\boldsymbol{V}}\boldsymbol{q}\rangle$	-54.5 (-96.6)	272.4 (260.4)	222.9	0.66

Table 3. Same as Table 1 except for the Fall non-precipitation period.

	mean	std	rmse	corr
R_{TOA}-R_{SRF}	-113.6(-106.3)	65.4 (93.2)	35.8	0.96
L*PREC	0.83 (0)	2.9 (0)	3.1	N/A
SH	8.2 (12.5)	66.2 (68.8)	37.6	0.84
$L*E_s$	26.9 (14.8)	38.6 (18.3)	26.8	0.88
$C_p*\partial\langle \boldsymbol{T} \rangle/\partial \boldsymbol{t}$	-32.6(-37.9)	256.7 (294.5)	104.8	0.94
$C_p*\langle \nabla \cdot \vec{\boldsymbol{V}}\boldsymbol{T} \rangle$	-71.6 (-55.9)	224.7 (295.4)	117.9	0.93
$L*\partial\langle \boldsymbol{q} \rangle/\partial \boldsymbol{t}$	-24.9(-16.7)	171.0 (131.2)	80.2	0.89
$L*\langle \nabla \cdot \vec{\boldsymbol{V}}\boldsymbol{q} \rangle$	51.1 (31.7)	163.2 (126.5)	81.2	0.88

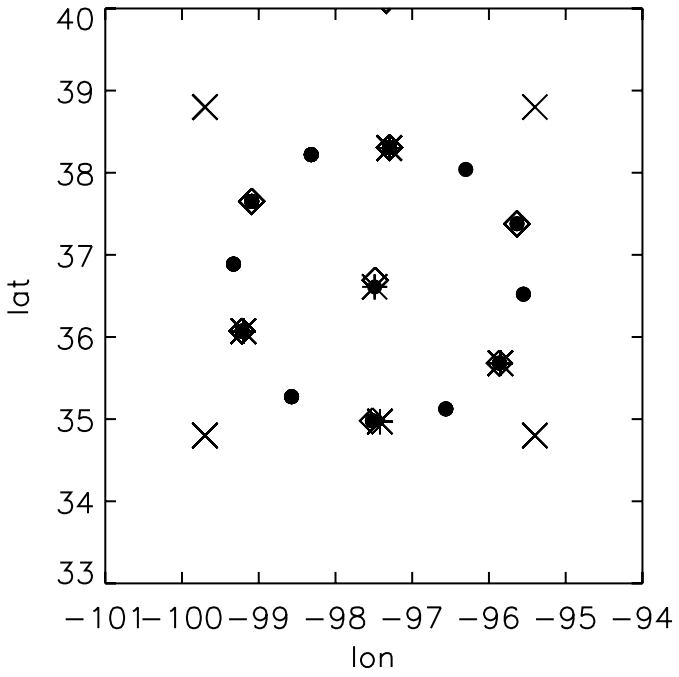

Figure 1

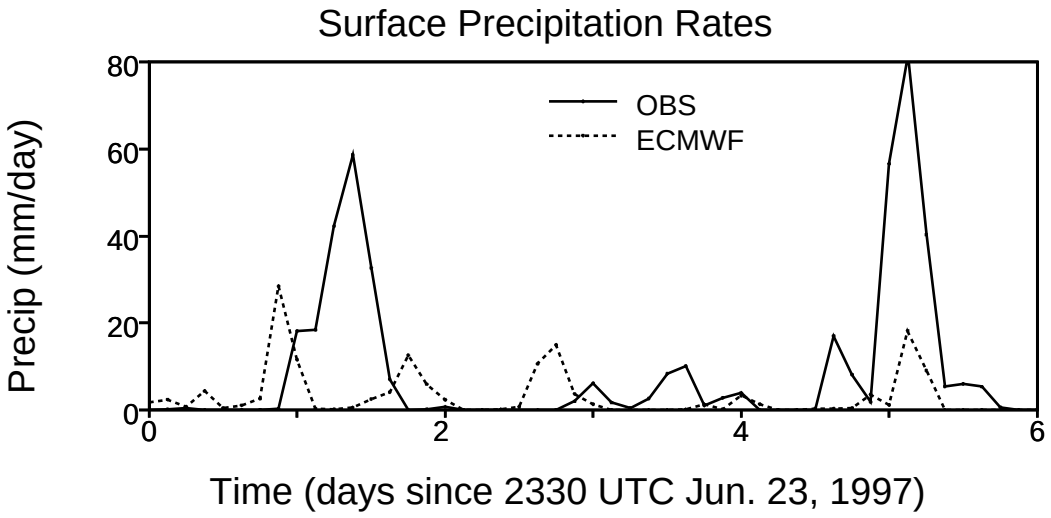
Surface Precipitation Rates
Precip (mm/day)
80
60
40
20
0
0
2
4
6
OBS
ECMWF
Time (days since 2330 UTC Jun. 23, 1997)

Figure 2

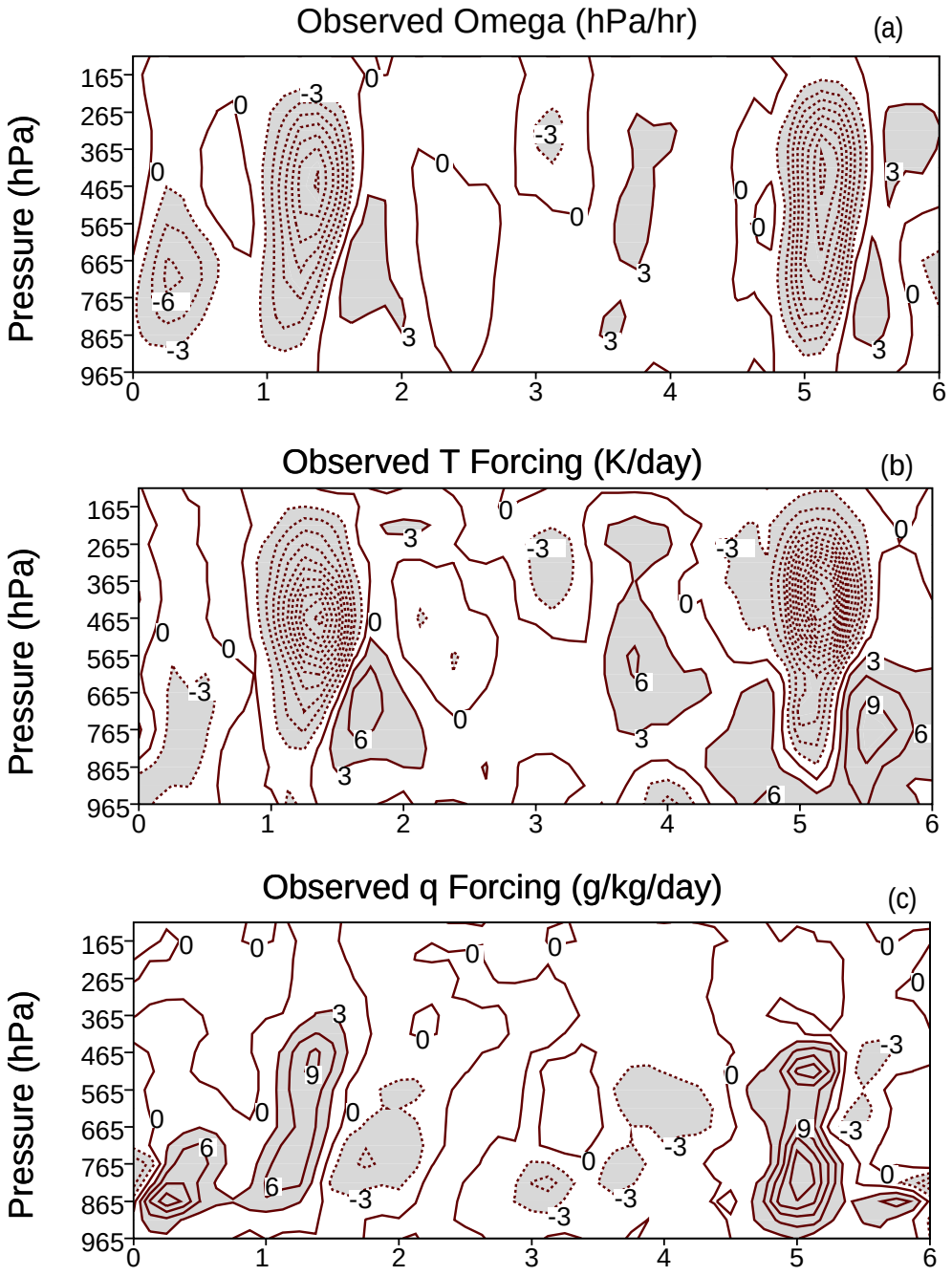
Observed Omega (hPa/hr)
(a)
Observed T Forcing (K/day)
(b)
Observed q Forcing (g/kg/day)
(c)
Pressure (hPa)
165
265
365
465
565
665
765
865
965
0
1
2
3
4
5
6
Time (days since 2330 UTC Jun. 23, 1997)

Figure 3

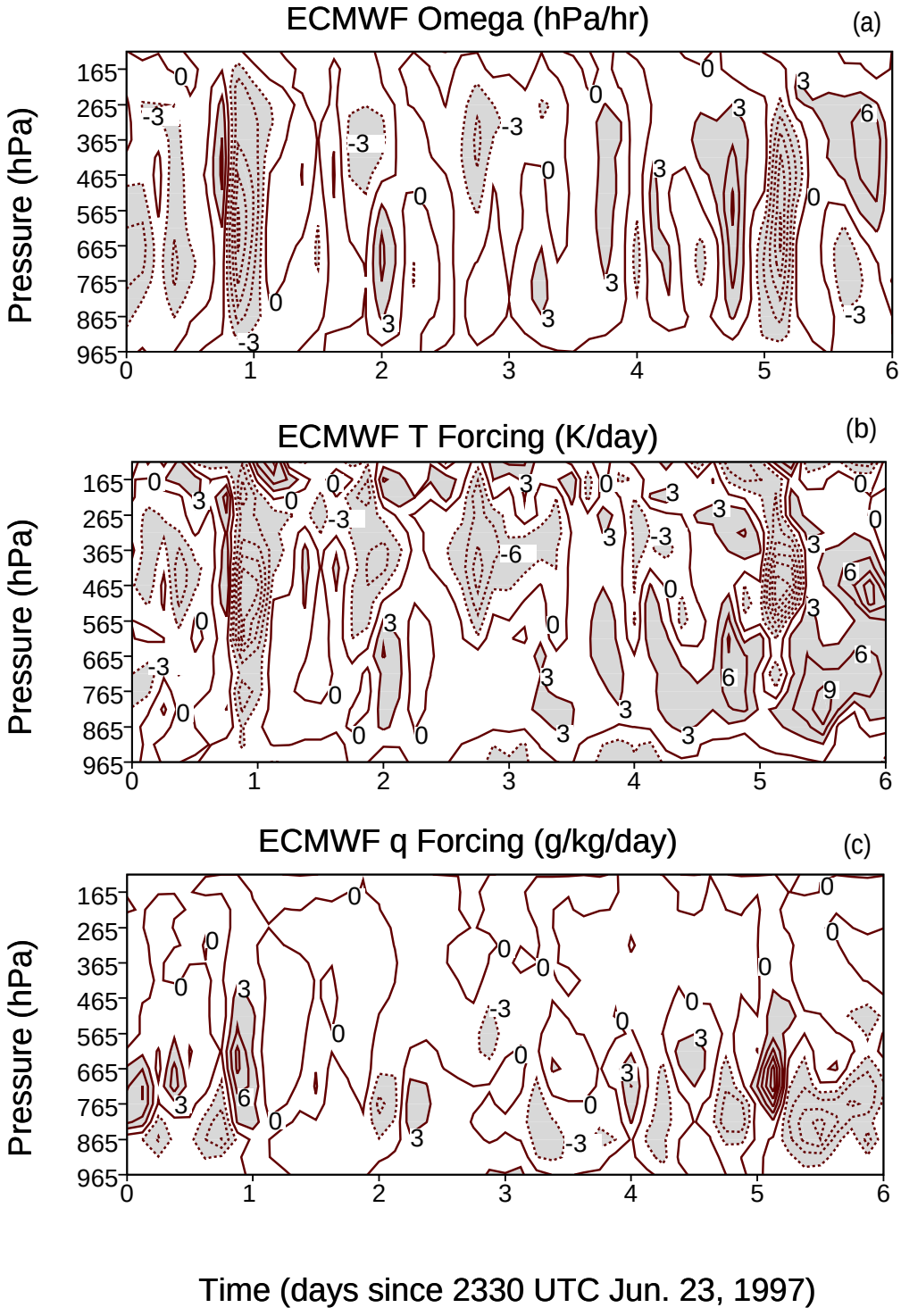
ECMWF Omega (hPa/hr)
(a)
ECMWF T Forcing (K/day)
(b)
ECMWF q Forcing (g/kg/day)
(c)
Pressure (hPa)
165
265
365
465
565
665
765
865
965
0
1
2
3
4
5
6
Time (days since 2330 UTC Jun. 23, 1997)

Figure 4

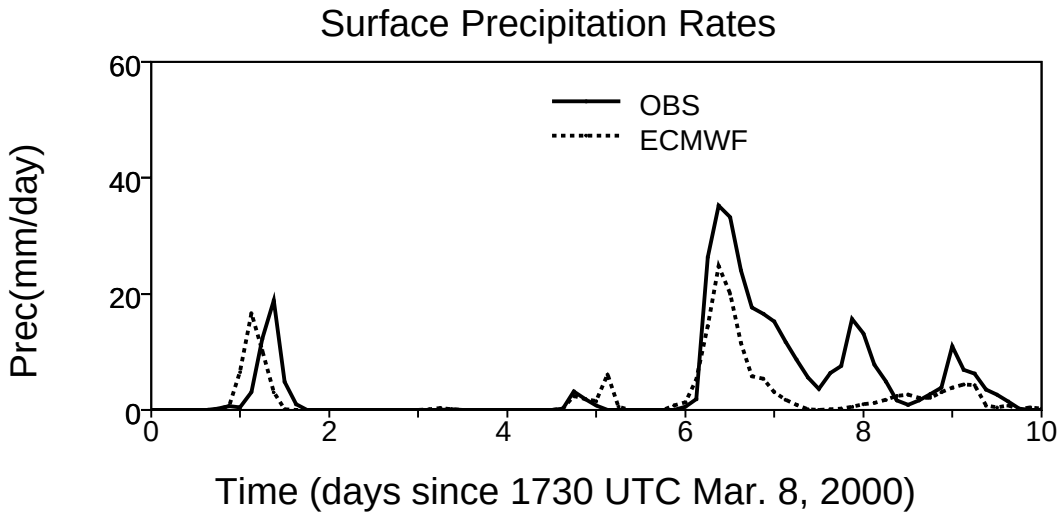
Surface Precipitation Rates
Prec(mm/day)
60
40
20
0
OBS
ECMWF
0
2
4
6
8
10
Time (days since 1730 UTC Mar. 8, 2000)

Figure 5

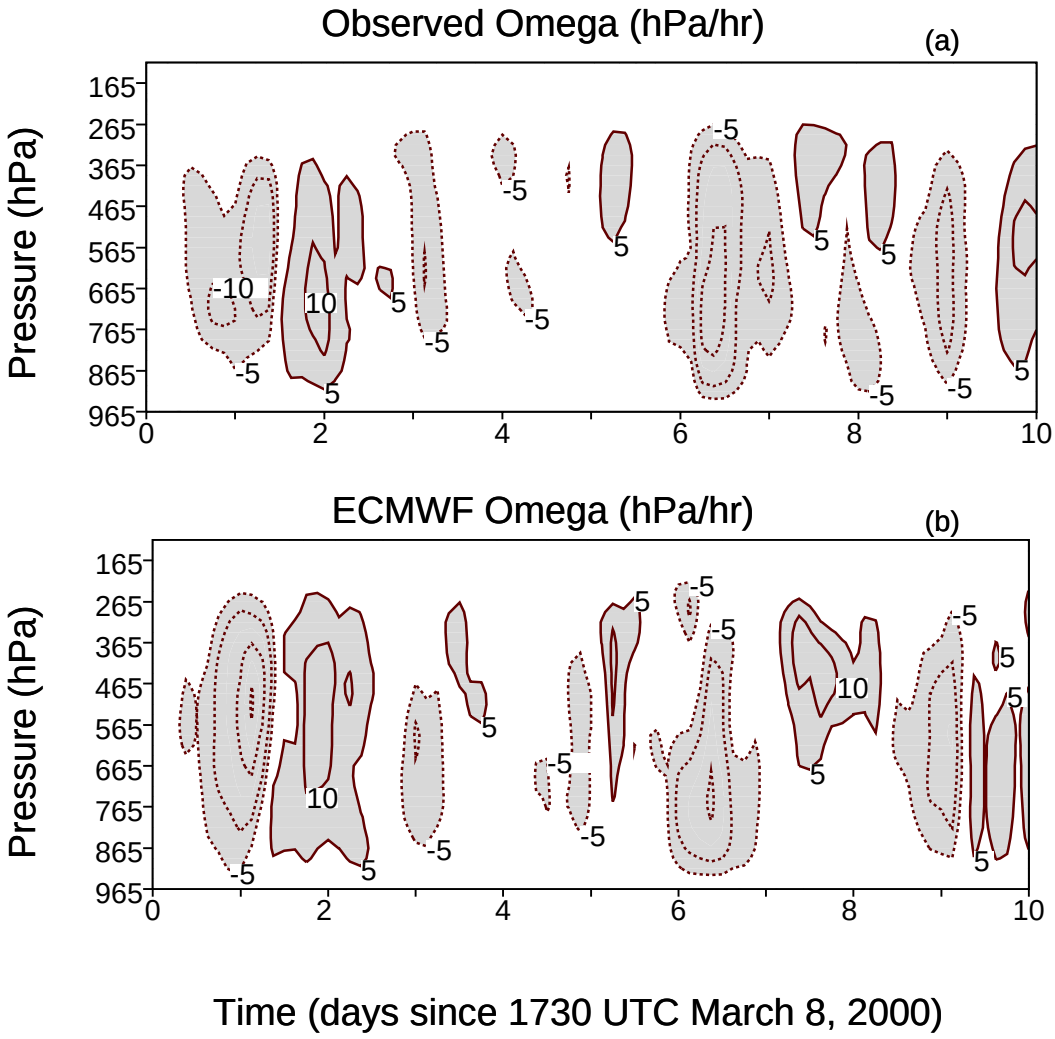
Observed Omega (hPa/hr)
(a)
Pressure (hPa)
165
265
365
465
565
665
765
865
965
0
2
4
6
8
10
-10
10
-5
5
ECMWF Omega (hPa/hr)
(b)
Pressure (hPa)
Time (days since 1730 UTC March 8, 2000)

Figure 6

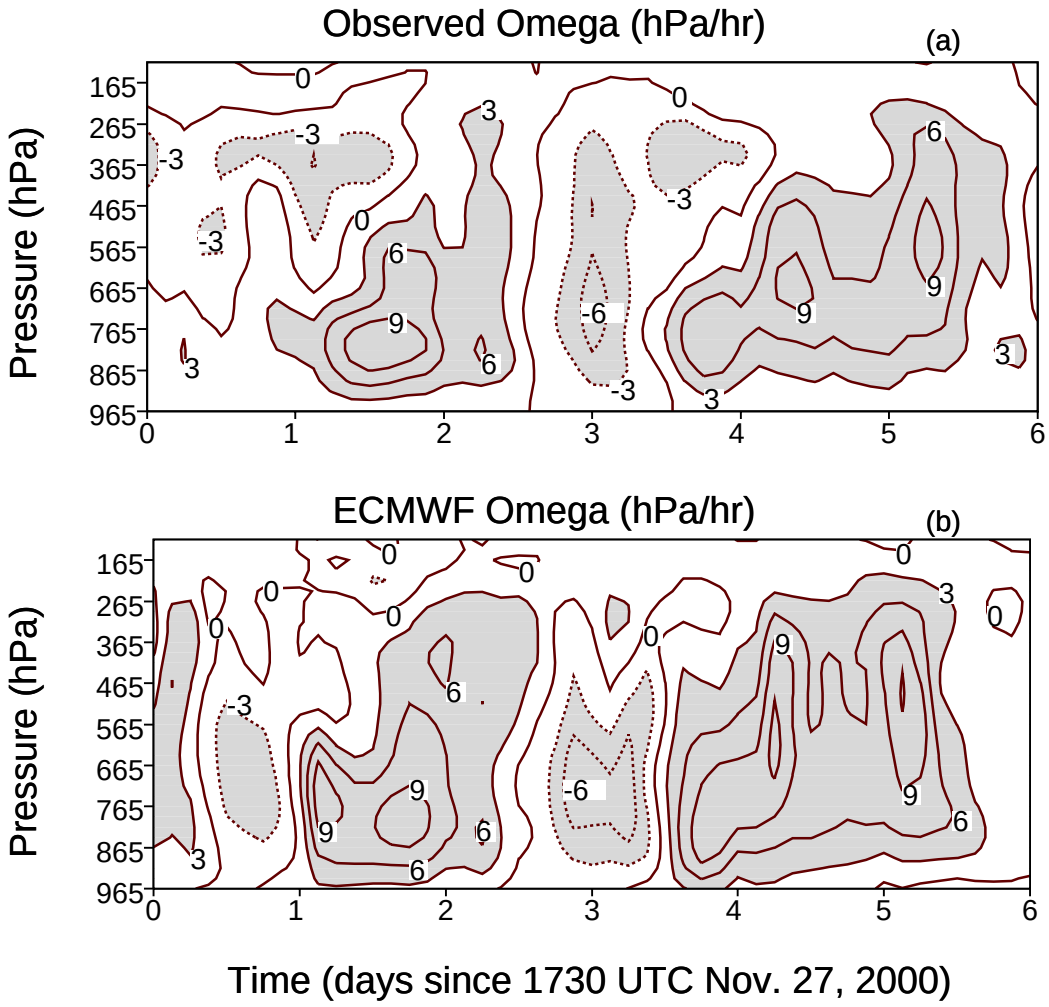
Observed Omega (hPa/hr)
(a)
Pressure (hPa)
165
265
365
465
565
665
765
865
965
0
1
2
3
4
5
6
ECMWF Omega (hPa/hr)
(b)
Pressure (hPa)
Time (days since 1730 UTC Nov. 27, 2000)

Figure 7

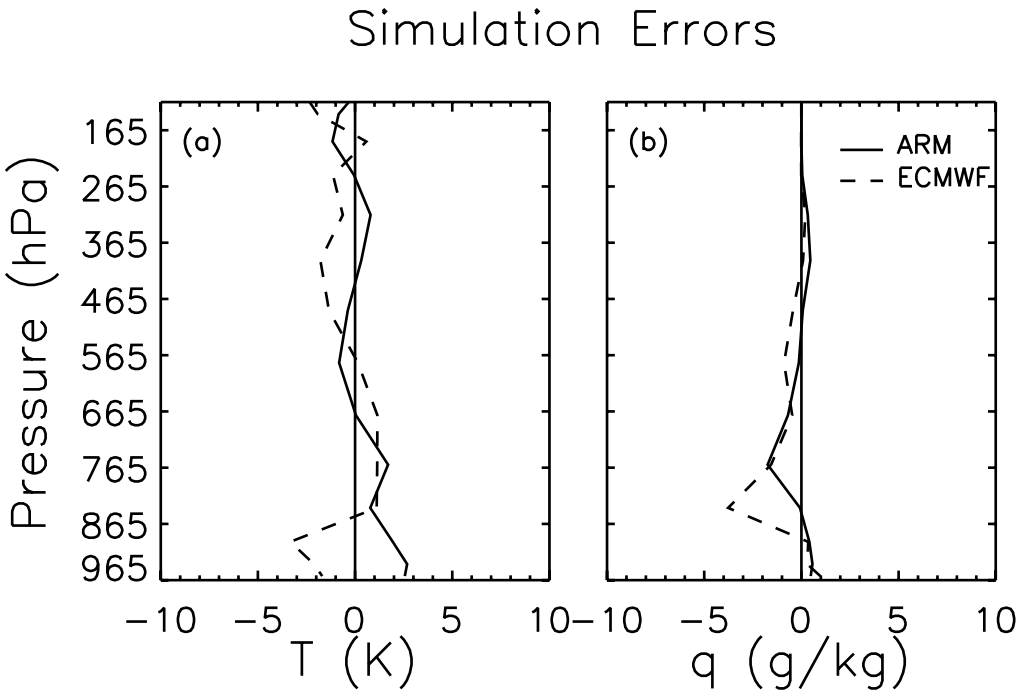
Simulation Errors
Pressure (hPa)
165
265
365
465
565
665
765
865
965
(a)
(b)
ARM
ECMWF
−10
−5
0
5
10
T (K)
q (g/kg)

Figure 8

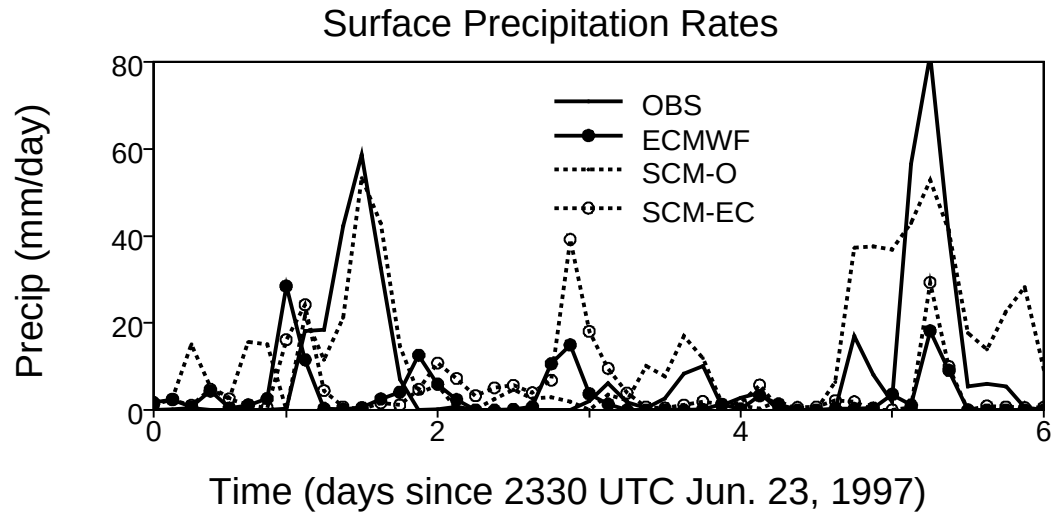

Figure 9

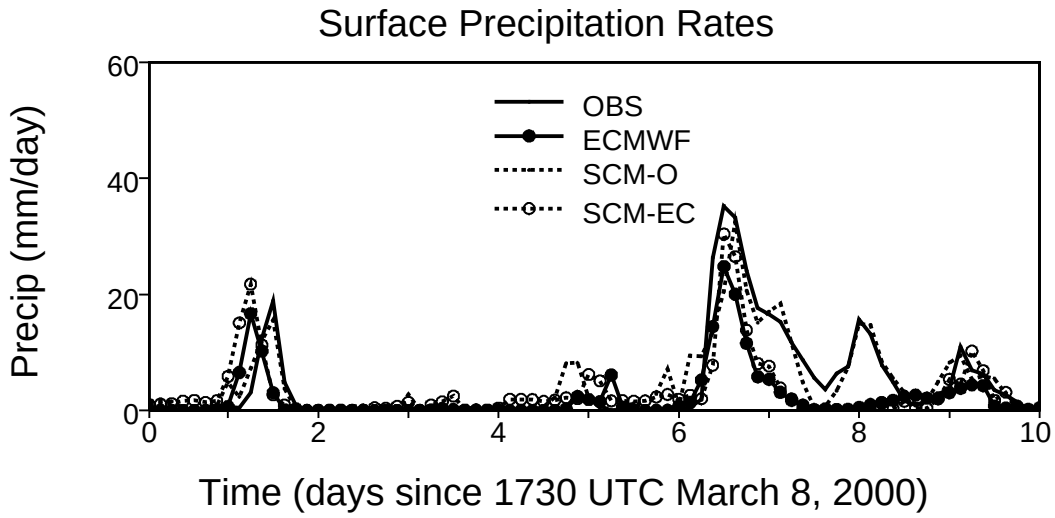

Figure 10

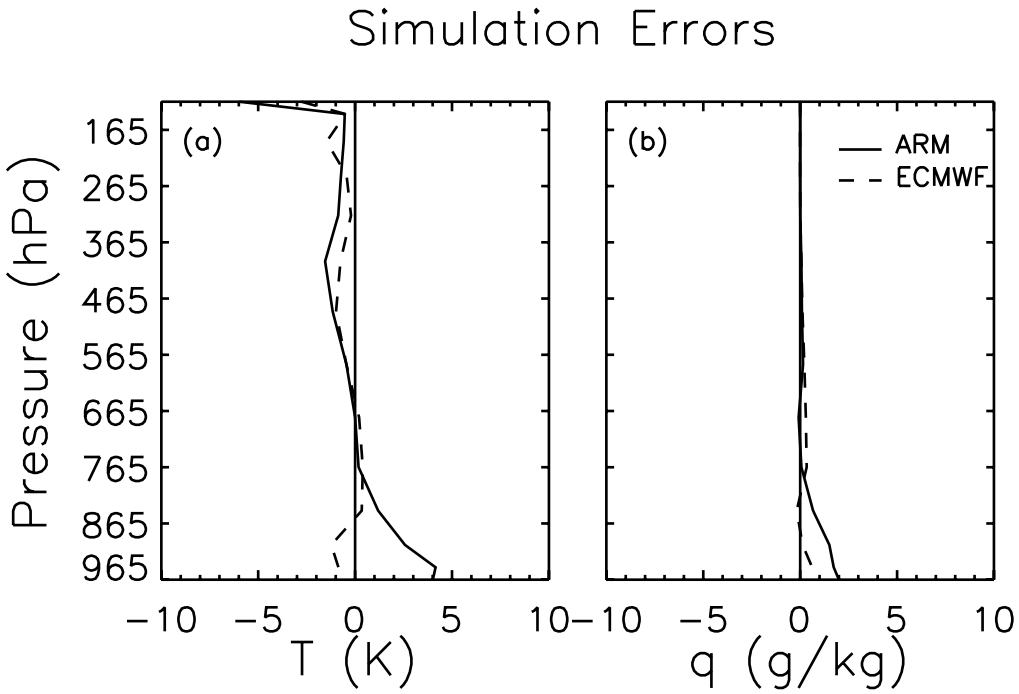
Simulation Errors
Pressure (hPa)
165
265
365
465
565
665
765
865
965
(a)
(b)
ARM
ECMWF
−10
−5
0
5
10
T (K)
q (g/kg)

Figure 11

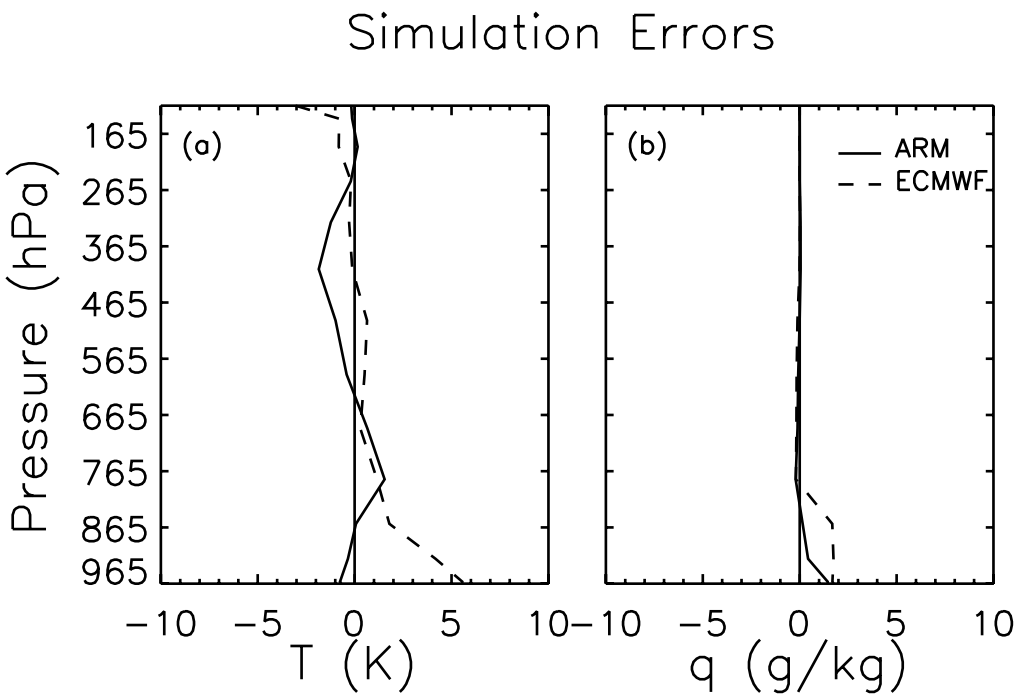
Simulation Errors
(a)
(b)
ARM
ECMWF
Pressure (hPa)
165
265
365
465
565
665
765
865
965
−10
−5
0
5
10
T (K)
q (g/kg)

Figure 12